



Full Length Article

Interface modification of an Al current collector for ultrafast lithium-ion batteries

Dong-Yo Shin^a, Dong-Hyoek Park^b, Hyo-Jin Ahn^{a,b,*}^a Program of Materials Science & Engineering, Convergence Institute of Biomedical Engineering and Biomaterials, Seoul National University of Science and Technology, Seoul 01811, Republic of Korea^b Department of Materials Science and Engineering, Seoul National University of Science and Technology, Seoul 01811, Republic of Korea

ARTICLE INFO

Keywords:

Ultrafast Lithium ion batteries
Aluminum current collector
Interface modification
Cathode
Electrochemical etching

ABSTRACT

The ability to provide a reasonable design and a practical modification of the interfacial structure in lithium-ion batteries (LIBs) is a key technology to enhance electrochemical kinetics and to improve ultrafast cycling performances. However, in recent years, despite considerable structural engineering efforts focused on active materials, in practice, ultrafast LIB performances still are characterized by low ultrafast cycling capacity and poor stability at the current density above 6 C. To solve these problems, in the present study, we propose a unique interface modification of the Al foil having crater porous interface using the electrochemical etching process. The cathode fabricated with a crater porous interface of the Al foil exhibits a remarkably enhanced ultrafast storage performance, such as high ultrafast cycling capacity (91.0 mAh g^{-1} at 10 C) and superb ultrafast cycling stability (76.2 mAh g^{-1} with the capacity retention of 84.8% at 10 C after 250 cycles) as compared to those of the cathode fabricated with the bare Al foil and commercial-etched Al foil. These improved electrochemical performances can be explained by the combined effects of improved electrical conductivity related to fast charge transport and increased interface contact area between the active material and the current collector related to enhanced interface adhesion during ultrafast cycling performance.

1. Introduction

In recent years, lithium-ion batteries (LIBs) have been widely applied in various portable electronic devices, such as, among others, laptops, smart watches, smartphones, and tablet PCs. Due to their higher energy density, longer life times, greater environmental friendliness, and no memory effect as compared to commercial secondary batteries (e.g. lead acid batteries, NiCd batteries, and NiMH batteries), LIBs have a great potential [1–3]. However, despite the increasing use and consumption of LIBs, their development for the use in high technology devices (such as electrical vehicles, military drones, and power assist suits) is still limited due to their poor ultrafast cycling performance, such as a slow charge time, a low cycling stability, and a poor ultrafast cycling capacity [4,5]. To overcome these problems, structural design of electrode materials, development of electrolytes with additive, and interface engineering of components in electrode have been continually studied [6,7]. Among proposed strategies, interface engineering has received a considerable research attention, as it is a key technology that can determine the electrical, mechanical, optical, and

electrochemical properties by unique structures and geometric architectures [8]. In addition, interface engineering through interface modification could improve the ultrafast cycling performances owing to the enhanced ionic and electronic behaviors. Specifically, in recent years, interface modification between the cathode material and the current collector has intensively emerged as an excellent promising and attractive approach to more effectively improve electrical conductivity, ion/electron transport ability, and interfacial stability [8]. However, most previous studies on interface engineering have been conducted on the interface between active materials and the electrolyte [9,10]. By contrast, studies on interface modification occurring between the active materials and the current collector are scarce, although the interface modification is an essential important factor to retain a high electrical conductivity and a good adhesion [8,11].

In the present study, we propose a unique interface modification having crater porous interface on the Al foil in the cathode for ultrafast LIBs. The crater porous interface of Al foil was fabricated using the electrochemical etching process which can adjust the morphology (pore size, depth, and uniformity) of pores on current collector interface,

* Corresponding author at: Department of Materials Science and Engineering, Seoul National University of Science and Technology, Seoul 01811, Republic of Korea.

E-mail address: hjahn@seoultech.ac.kr (H.-J. Ahn).

unlike a commercial acid etching process.

2. Experiments

The Al foil with the crater porous interface in the cathode of LIBs was successfully fabricated using the electrochemical etching process. To fabricate the crater porous interface, bare Al foil (99.8%, MTI Corp.) was electrochemically etched in the mixed solution of nitric acid (HNO_3 , 66%, SAMCHUN) and hydrofluoric acid (HCl, 52%, SAMCHUN) in DI-water. The electrochemical etching process was performed using a potentiostate/galvanostat (PGST302N by Eco Chemie, Netherlands) using a conventional three-electrode system composed of a Pt gauze as the counter electrode, Ag/AgCl (saturated in KCl) as the reference electrode, and a bare Al foil as the working electrode. During the electrochemical etching process, the applied voltage was maintained at 0.5 V for 30 s to form the crater porous structure on the bare Al foil surface. The Al foil with the crater porous interface is henceforth referred to as crater porous Al foil.

The surface morphology and roughness of the samples were demonstrated using field-emission scanning electron microscopy (FESEM, Hitachi S-4700) and atomic electron microscopy (AFM, diDimension™ 3100). The electrical conductivity of the samples was examined using the Hall measurement technique (Ecopia, HMS-3000). Thereafter, in order to measure the electrochemical properties, the electrode was prepared using coin-type cells (CR2032, Hohsen Corp.). The coin-type cells are composed of a cathode and an anode (Li metal foil, 99.8%, Honjo Chemical) as electrodes, a LiPF_6 solution with a mixture of ethylene carbonate and dimethyl carbonate (1:1) as the electrolyte, and a porous polypropylene membrane (Celgard 2400) as the separator. The cathode was prepared by coating the crater porous Al foil with the slurry composed of 70 wt% lithium cobalt oxide (LiCoO_2 , 99.8%, Sigma-Aldrich) as the active material, 20 wt% polyvinylidene fluoride as the binder, and 10 wt% ketjen black as the conducting material in N-methyl-2-pyrrolidone. In addition, to investigate the effect of crater porous Al foil, the slurry was coated on bare Al and commercial-etched Al foil (20 μm , > 99.7%, JCC Korea Co.). Henceforth, the cathodes fabricated with the bare Al foil, commercial-etched Al foil, and crater porous Al foil are referred to as sample A, sample B, and sample C, respectively. The resultant cathodes were dried at 100 °C for 12 h in a convention oven. All coin-type cells were then assembled using an argon-filled glove box with the H_2O and O_2 content below 5 ppm. In order to investigate the electrochemical performance of all electrodes, the cycling performance was measured in the potential range of 3.0–4.2 V (versus Li/Li⁺) using a battery cycler system (WonATech Corp., WMPG 3000). The cycling stability was performed up to 100 cycles at the current density of 1 C. The C-rate performance was measured at the current densities of 1 C, 3 C, 5 C, 7 C, and 10 C. The ultrafast cycling performance was carried out up to 250 cycles at the current density of 10 C. In addition, the electrochemical kinetics of all electrodes was inspected by electrochemical impedance spectroscopy (EIS) measurement in the frequency range of 10^5 to 10^{-2} Hz using an AC signal of 5 mV.

3. Results and discussion

Fig. 1 shows the top-view (**Fig. 1a–c**) and the cross-view (**Fig. 1d–f**) FESEM images of bare Al foil, commercial-etched Al foil, and crater porous Al foil, respectively. Bare Al foil (see **Fig. 1a**) had a smooth surface morphology. On the other hand, the commercial-etched Al foil exhibited a porous surface morphology, consisting of nano-sized pores and micro-sized pores with the diameters of 80.1–360.4 nm and 3.1–4.8 μm , respectively (see **Fig. 2b**). The micro-sized pores of commercial-etched Al foil were made by agglomerated nano-sized pores on surface. However, the crater porous Al foil showed uniform crater pores of 1.1–2.8 μm in diameter (see **Fig. 2c**). Furthermore, it is well known that the Al_2O_3 film with the thickness of 20–100 Å, having a high chemical/

physical stability and a low electrical conductivity, is formed on the Al foil surface owing to the pollution in air [12]. However, the Al_2O_3 film is removed using the supplied potential in the range from –1.3 to 1.2 V in acidic atmosphere under pH 4 [12,13]. This is so because, according to potential-pH diagram of Al-H₂O system, the Al_2O_3 is transformed to stable Al^{3+} state in atmosphere under pH 4 with potential of –0.5 V by phase transformation. Then, crater-like pores are formed by a partial decomposition of Al^{3+} in acid solution according to chemical reactions (1) and (2) [13].



Therefore, the crater pores formed on surface can provide the high interface contact area between the active material and the current collector related to the improvement of interfacial reaction with interface adhesion.

To demonstrate the surface roughness of the samples, AFM analyses were performed. **Fig. 2a–c** shows the AFM images obtained from bare Al foil, commercial-etched Al foil, and crater porous Al foil. The height roughness (R_a) means the average height value of the surface based on the center, corresponding to height roughness and the interface width [14]. The R_a values of bare Al foil, commercial-etched Al foil, and crater porous Al foil are 24.0 nm, 136.8 nm, and 193.7 nm, respectively. These results mean that the crater pores formed on the surface can effectively increase the surface roughness, which is related to the improvement of the interface contact area, together with a uniform formation of crater pores of 1.1–2.8 μm in diameter.

Furthermore, to investigate the electrical conductivity of the samples according to surface morphology, the Hall effect measurement was performed (see **Fig. 2d**). Due to the Al_2O_3 film having a high electrical resistance on the Al surface, the electrical conductivity of bare Al foil displayed the lowest value of 1.20 S cm⁻¹. On the other hand, electrical conductivity of commercial-etched Al foil exhibited a relatively low value of 1.28 S cm⁻¹, since the Al_2O_3 film was not fully removed on commercial-etched Al foil. In addition, the nano-sized pores of surface and interior decreased the movement of electrons by reduction of the electron pathway [15,16]. Among the samples, due to the removal of the Al_2O_3 film, crater porous Al foil had the highest electrical conductivity of 1.34 S cm⁻¹. In this respect, the increased electrical conductivity of crater porous Al foil can effectively provide a fast electron transfer.

Fig. 3 shows the cross-section view of samples A–C. All electrodes were prepared by coating on the surface of bare Al foil, commercial-etched Al foil, and crater porous Al foil with the slurry consisting of the active material. In **Fig. 3a–c**, based on the white line, the top section shows the active material and the bottom section shows the current collector. In **Fig. 2b**, due to the existence of nano-sized pores on the surface and interior of commercial-etched Al foil, the active material is not fully covered on surface and inside of current collector of sample B [17]. However, the sample C exhibits the fully and uniformly covered interface with active material along the etched pattern. These results mean that the size of pores can affect the coverage uniformity of the active material on interface of current collector [18]. Furthermore, the adhesion strength of sample C (4175 mN) showed a higher than sample A (3796 mN) due to the increased interface contact area between the active material and the current collector. The enhanced adhesion strength can improve the ultrafast cycling performance in LIBs by superb interfacial stability between active material and current collector [17,18].

Fig. 4a shows the cycling stability tests of all electrodes at the current density of 1 C up to 100 cycles. Sample A presents a drastic drop in the specific capacity to 84.5 mAh g⁻¹ after 100 cycles. For sample B, a relatively low specific capacity of 104.5 mAh g⁻¹ after 100 cycles was observed. These results indicate that a poor interface contact area causes a low cycling stability [17]. Sample C exhibits a high cycling

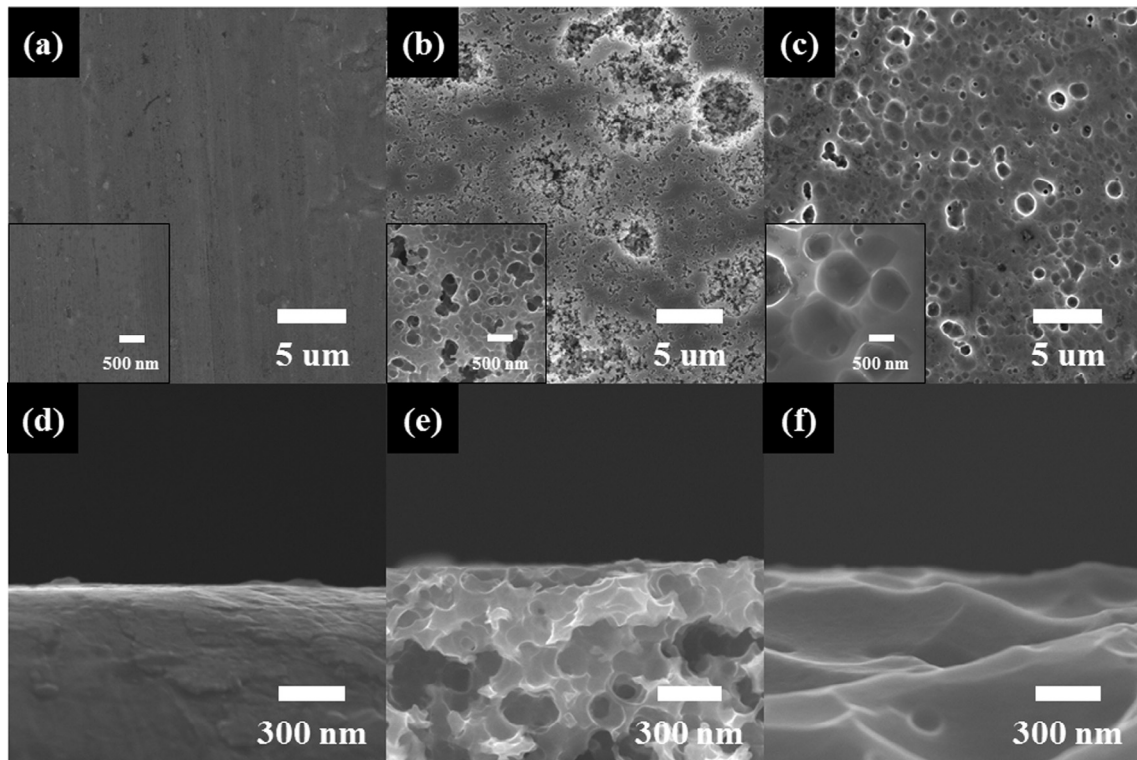


Fig. 1. (a–c) Top-view and (d–f) cross-view FESEM images of bare Al foil, commercial-etched Al foil, and crater porous Al foil.

stability (115.0 mAh g^{-1} after 100 cycles) due to a high interface contact area and a high interface adhesion between the active material and the current collector [8,18].

Fig. 4b shows the high-rate performances obtained from the current densities of 1 C, 3 C, 5 C, 7 C, 10 C, and 1 C, respectively. Sample C exhibited an excellent high-rate performance of 91.0 mAh g^{-1} at 10 C, which was recovered to 124.9 mAh g^{-1} with 99.7% of the specific capacity at 1 C. In addition, sample C exhibited the highest ultrafast cycling capacity of 76.2 mAh g^{-1} with the superb ultrafast cycling stability of 84.8% after 250 cycles (see Fig. 4c) among the samples. The improved C-rate and ultrafast cycling performances can be attributed to the combined effect of the enhanced electrical conductivity arising from removed Al_2O_3 film due to a fast electron transport during the cycling performance, one the one hand [12,13], and the high interface contact area with interface adhesion between the active material and the current collector by crater porous structure [8,17].

To further investigate the electrochemical kinetics relative to Li^+ diffusion process, electrochemical impedance spectroscopy (EIS) analyses were carried out (see Fig. 4d). In the high-frequency region, the semicircle showed the information of bulk resistance (R_{sol}), ionic

resistance (R_{ion}), and charge transfer resistance (R_{ct}). Especially, the small semicircle size is caused by low R_{ct} related to low charge transfer resistance at the interface of electrode-electrolyte. In the low-frequency region, the inclined line means Li^+ diffusion (called also the Warburg impedance) [4,7]. Sample C had the lowest R_{ct} with the lowest Warburg impedance among the samples. The low R_{ct} of the sample C can be attributed to the high electrical conductivity based on the removal of Al_2O_3 film having a high electrical resistance [4,7]. The Warburg impedance of the sample C could be reduced owing to an increased interface contact area between the active material and the current collector [18]. In addition, the Li^+ diffusion coefficient of all samples could be calculated from the inclined line in low-frequency region according to Eqs. (3) and (4) [9].

$$Z_{\text{real}} = R_{\text{e}} + R_{\text{ct}} + \sigma_w \omega^{-1/2} \quad (3)$$

$$D = R^2 T^2 / 2 A^2 n^4 F^4 C^2 \sigma_w^2 \quad (4)$$

where σ_w , D, R, T, F, A, n, and C is the Warburg impedance coefficient, the Li^+ diffusion coefficient, the gas constant, the temperature, the Faraday constant, the electrode area, the number of electrons in

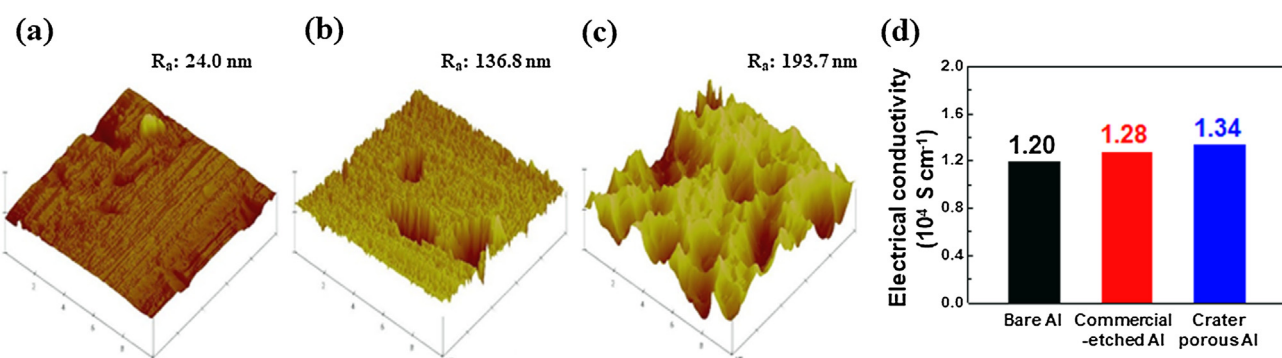


Fig. 2. AFM images of (a) bare Al foil, (b) commercial-etched Al foil, and (c) crater porous Al foil and (d) electrical conductivity of all current collectors.

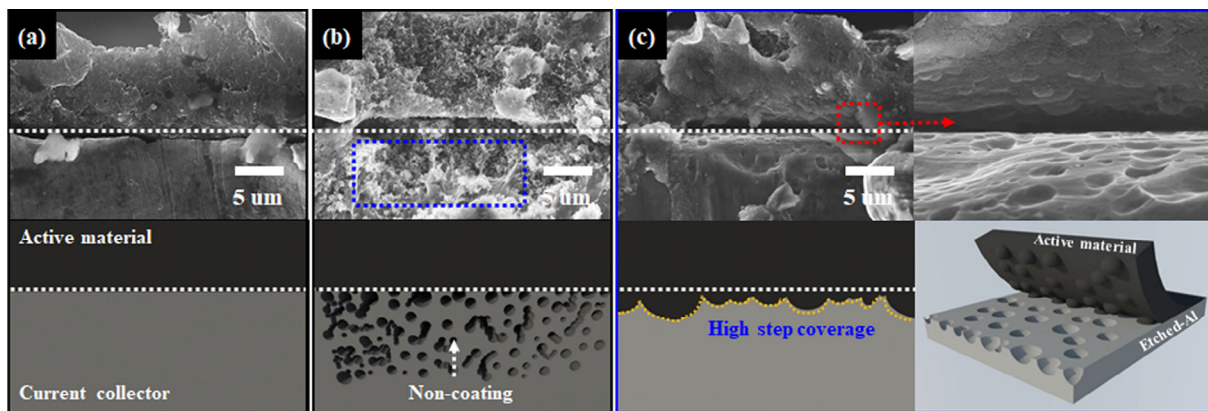


Fig. 3. Cross-view FESEM images of (a) sample A, (b) sample B, and (c) sample C fabricated of bare Al foil, commercial-etched Al foil, and crater porous Al foil.

molecule, and the molar concentration of Li^+ . Among the samples, the Li^+ diffusion coefficient of sample C showed the highest value ($3.3 \times 10^{-12} \text{ cm}^2 \text{ s}^{-1}$), indicating that their crater porous structure could efficiently enhance the Li^+ diffusion process during the ultrafast cycling performance due to the increased interface contact area with enhanced electrical conductivity between active materials and current collector (Fig. 4e–f) [18].

Therefore, in the present study, the improved electrochemical performances of sample C were achieved by interface modification of the Al foil. Thus, the enhanced ultrafast cycling performances can be attributed to two main effects. First, improvement of electrical conductivity enables an efficient electron transport, leading to increased ultrafast cycling capacity. Second, the enhancement of interface contact area between the active material and the current collector can yield excellent interface adhesion, leading to ultrafast cycling stability. These results demonstrate an excellent ultrafast cycling performance at a high-rate current density of 10 C (see Fig. 5).

4. Conclusions

In the present study, the Al foil with crater porous structure in the cathode for ultrafast LIBs were successfully fabricated using the electrochemical etching process. The crater porous Al foil indicated a crater

size in the range from 1.1 to 2.8 μm . Specifically, we proposed a unique interface modification of the Al foil. The considerably improved electrochemical performances of sample C with a good cycling stability (115.0 mAh g^{-1} at 1 C after 100 cycles), an excellent high-rate property (91.0 mAh g^{-1} at 10 C), and a superb ultrafast cycling stability (76.2 mAh g^{-1} at 10 C after 250 cycles) were investigated with respect to the following two main factors: (1) a high ultrafast cycling capacity is attributed to an improved electrical conductivity, which effectively provides an electron transport; (2) the superb ultrafast cycling stability is related to an increased interface contact area between the active material and the current collector, providing an enhancement of interface adhesion. Taken together, these results suggest that the interface modification of Al current collector in the cathode based on crater porous structure might be a promising strategy for practical applications of ultrafast LIBs.

Acknowledgement

This work was supported by the Technology Innovation Program (10080656, Development of ceramic/carbon convergence and integration anode material for 10 C fast charging Lithium ion battery) funded by the Ministry of Trade, Industry & Energy (MOTIE, Korea).

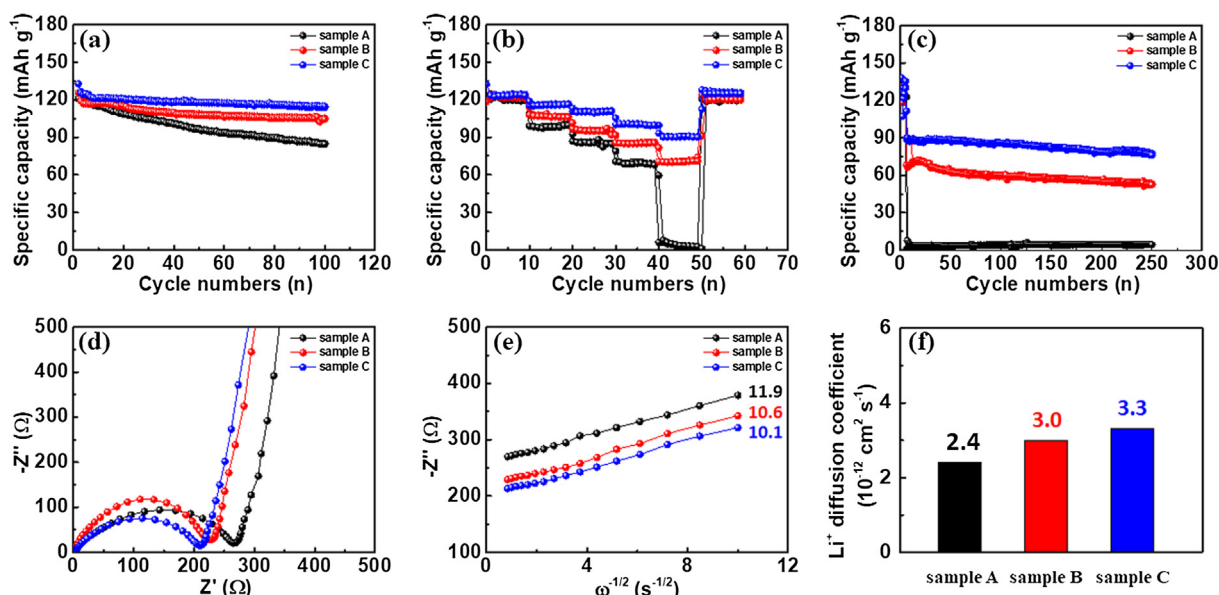


Fig. 4. (a) Cycling test at current density of 1 C up to 100 cycles, (b) rate-performance at current density of 1 C, 3 C, 5 C, 7 C, 10 C, and 1 C, (c) ultrafast cycling performance at 10 C up to 250 cycles, (d) Nyquist plots, (e) relationship between $\omega^{-1/2}$ and Z_{real} in the low frequency range of all electrodes, and (f) Li^+ diffusion coefficient of all electrodes calculated by EIS results.

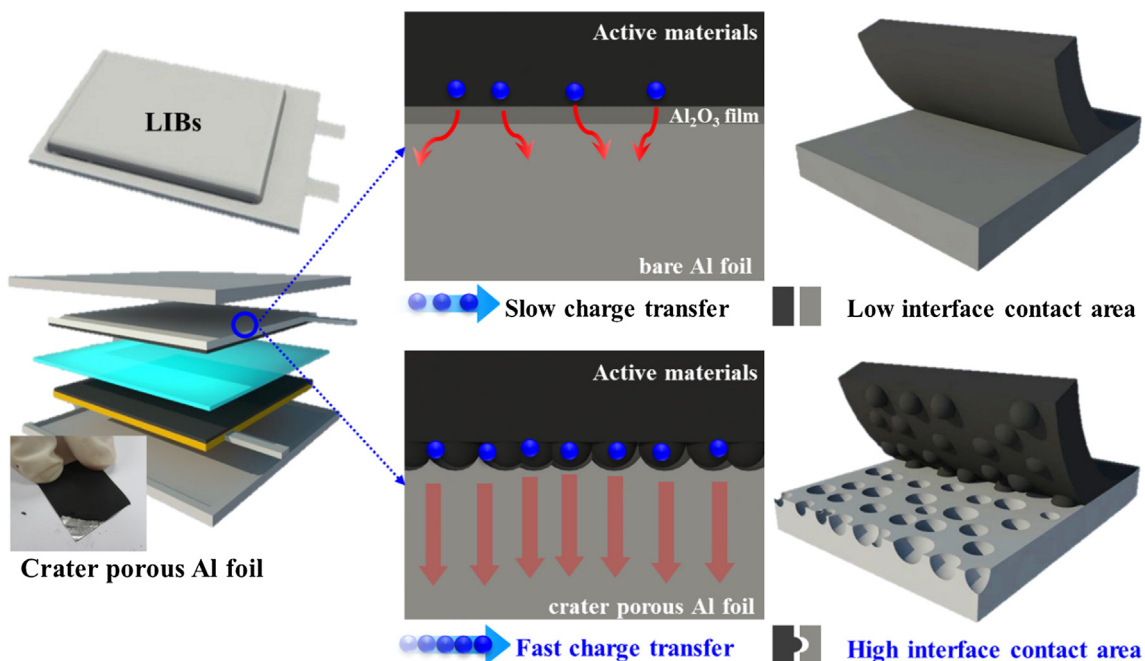


Fig. 5. Schematic illustration of the two main effects on the cathode fabricated with the bare Al foil and the crater porous Al foil for enhancing ultrafast cycling performances.

References

- [1] Y.M. Chen, X.Y. Yu, Z. Li, U. Paik, X.W. Lou, Hierarchical MoS₂ tubular structures internally wired by carbon nanotubes as a highly stable anode material for lithium-ion batteries, *Sci. Adv.* 2 (2016) 1–8.
- [2] N. Balke, S. Jesse, A.N. Morozovska, E. Eliseev, D.W. Chung, Y. Kim, L. Adamczyk, R.E. Garcia, N. Dudney, S.V. Kalinin, Nanoscale mapping of ion diffusion in a lithium-ion battery cathode, *Nat. Nanotechnol.* 5 (2010) 749–754.
- [3] S. Guo, Y. Chen, L. Shi, Y. Dong, J. Ma, X. Chen, H. Song, Nitrogen-doped biomass-based ultra-thin carbon nanosheets with interconnected framework for high-performance lithium-ion batteries, *Appl. Surf. Sci.* 437 (2018) 136–143.
- [4] G.H. An, D.Y. Lee, H.J. Ahn, Tunneled mesoporous carbon nanofibers with embedded ZnO nanoparticles for ultrafast lithium storage, *ACS Appl. Mater. Interf.* 9 (2017) 12478–12485.
- [5] S. Liu, H. Jia, L. Han, J. Wang, P. Gao, D. Xu, J. Yang, S. Che, Nanosheet-constructed porous TiO₂-B for advanced lithium ion batteries, *Adv. Mater.* 24 (2012) 3201–3204.
- [6] Y. Choi, J.I. Kim, J. Moon, J. Jeong, J.H. Park, Electron beam induced strong organic/inorganic grafting for thermally stable lithium-ion battery separators, *Appl. Surf. Sci.* 444 (2018) 339–344.
- [7] D.Y. Shin, Y.G. Lee, H.J. Ahn, One-pot synthesis of aluminum oxide coating and aluminum doping on lithium manganese oxide nanoparticles for high performance energy storage system, *J. Alloy Compd.* 727 (2017) 1165–1170.
- [8] Y.W. Lee, G.H. An, B.S. Kim, J. Hong, S. Pak, E.H. Lee, Y. Cho, J. Lee, P. Giraud, S.N. Cha, H.J. Ahn, J.I. Sohn, J.M. Kim, Synergistic effects of a multifunctional graphene based interlayer on electrochemical behavior and structural stability, *ACS Appl. Mater. Interf.* 8 (2016) 17651–17658.
- [9] G.H. An, H. Kim, H.J. Ahn, Improved ionic diffusion through the mesoporous carbon skin on silicon nanoparticles embedded in carbon for ultrafast lithium storage, *ACS Appl. Mater. Interf.* 10 (2018) 6235–6244.
- [10] F. Zou, X. Hu, Z. Li, L. Qie, C. Hu, R. Zeng, Y. Jiang, Y. Huang, MOF-derived porous ZnO/ZnFe₂O₄/C octahedral with hollow interiors for high-rate lithium-ion batteries, *Adv. Mater.* 26 (2014) 6622–6628.
- [11] G.H. An, D.Y. Lee, Y.J. Lee, H.J. Ahn, Ultrafast lithium storage using antimony-doped tin oxide nanoparticles sandwiched between carbon nanofibers and a carbon skin, *ACS Appl. Mater. Interf.* 8 (2016) 30264–30270.
- [12] R.S. Kuhnel, N. Bockenfeld, S. Passerini, M. Winter, A. Baldacci, Mixtures of ionic liquid and organic carbonate as electrolyte with improved safety and performance for rechargeable lithium batteries, *Electrochim. Acta* 56 (2011) 4092–4099.
- [13] H.T. Teng, T.Y. Lee, Y.K. Chen, H.W. Wang, G. Cao, Effect of Al(OH)₃ on the hydrogen generation of aluminum-water system, *J. Power Sources* 219 (2012) 16–21.
- [14] B.R. Koo, D.H. Oh, D.H. Riu, H.J. Ahn, Improvement of transparent conducting performance on oxygen activated fluorine-doped tin oxide electrode formed by horizontal ultrasonic spray pyrolysis deposition, *ACS Appl. Mater. Interf.* 9 (2017) 44584–44592.
- [15] J.K. Carson, S.J. Lovatt, D.J. Tanner, A.C. Cleland, Thermal conductivity bounds for isotropic porous materials, *Int. J. Heat Mass Transf.* 48 (2005) 2150–2158.
- [16] J. Wang, J. Yuan, B. Sundén, On electric resistance effects of non-homogeneous GDL deformation in a PEM fuel cell, *Int. Hydrog. Energy* 42 (2017) 28537–28548.
- [17] H.C. Wu, E. Lee, N.L. Wu, T.R. Jow, Effects of current collectors on power performance of Li₄Ti₅O₁₂ anode for Li-ion battery, *J. Power Sources* 197 (2012) 301–304.
- [18] C. Portet, P.L. Taberna, P. Simon, E. Flahaut, Modification of Al current collector/active material interface for power improvement of electrochemical capacitor electrodes, *J. Electrochem. Soc.* 154 (2006) A649–A653.